

Simulations of the Atmospheric Response to South Atlantic Sea Surface Temperature Anomalies

Andrew W. Robertson

International Research Institute for Climate Prediction, Palisades, NY

John D. Farrara and Carlos R. Mechoso

Department of Atmospheric Sciences, University of California, Los Angeles,

Los Angeles, California

March 29, 2002

J. Climate, to be submitted

Correspondence address:

Dr. Andrew W. Robertson
International Research Institute for Climate Prediction
PO Box 1000
Palisades, NY 10964
Tel: (845) 680 4491
Fax: (845) 680 4865
E-mail: awr@iri.columbia.edu

Abstract

The sensitivity of the atmospheric circulation to sea surface temperature (SST) anomalies over the tropical and subtropical South Atlantic is studied by means of simulations with an atmospheric general circulation model (GCM). Two cases are considered depending upon the prescribed SST anomalies. The first is observed to occur during austral summers in association with a strengthening of the South Atlantic Convergence Zone (SACZ), and consists of cold SST anomalies over the subtropical South Atlantic. The second is the leading seasonally varying empirical orthogonal function of SST, consisting of warm basin-scale anomalies with maximum amplitude in the subtropics during January–March and at the equator in June. An ensemble of about 10 seasonal simulations is made using each type of anomaly, focusing on the January–March period in the first case, and the January–June seasonal evolution in the second.

In the first case, cold subtropical SST anomalies during January–March are found to cause a strong statistically significant cooling in the lower troposphere, a net heat flux into the ocean and reduced rainfall over the maritime part of the SACZ, accompanied by anticyclonic lower-tropospheric wind anomalies in the SACZ region. There are no statistically significant anomalies in the upper troposphere.

In the second case, warm basin-scale anomalies are found to have their largest impact during boreal summer, with a strong statistically significant equatorial “Gill-type” response and positive rainfall anomalies over the equatorial ocean. The latter does not extend appreciably into the adjacent continents, although there are significant positive rainfall anomalies over the Sahel in April–June and negative anomalies over the western

Indian Ocean. In the upper troposphere, a statistically significant wave train extends southwestward to southern South America and northeastward to Europe in April–June.

1. Introduction

The tropical Atlantic Ocean is arguably second only to the tropical Pacific in the strength of its influence on the atmosphere on seasonal-to-interannual time scales, and the potential importance of this influence for predicting seasonal rainfall in tropical South America and Africa (e.g. Moura and Shukla 1981, Chang et al. 2000). The inter-tropical convergence zone (ITCZ) over the Atlantic migrates with the seasons and is modulated in its intensity and geographical area, extending its influence into northeast Brazil at its southernmost position during March–April, and Sahelian Africa as it migrates to its northernmost point in late boreal summer. Both of these regions experience significant droughts when the seasonal migration fails to be as pronounced as usual, or when there are anomalies in the ITCZ’s intensity and spatial extent (Hastenrath and Heller 1977, Lamb 1978a,b, Folland et al. 1991).

The ocean plays a key role in the scientific rationale behind seasonal-to-interannual climate prediction due to its large thermal inertia and slow dynamical adjustment times have the potential to influence the atmosphere. It is clear that the tropical Atlantic exerts a powerful control on the seasonal migration of the ITCZ because the latter lags the solar calendar by up to 3–4 months. The way in which interannual anomalies in Atlantic SSTs and coupled ocean-atmosphere interactions influence the ITCZ, particularly over the South Atlantic, is a matter of current debate. The dynamics of tropical Atlantic variability has often been described in terms of two modes: an equatorial mode with dynamics similar to those of the El Niño-Southern Oscillation (ENSO), but highly damped (Zebiak 1993, Tseng and Mechoso 2000), and a cross-equatorial “dipole”

mode (Chang et al. 1997). Recent work has demonstrated, however, that Atlantic SST anomalies are almost uncorrelated across the equator (Dommenget and Latif 2000). Several studies have addressed the tropical North Atlantic, which directly impacts the ITCZ and which is strongly influenced by ENSO in boreal spring (Enfield and Mayer 1997, Saravanan and Chang 2000), and by the North Atlantic Oscillation (NAO) (Namias 1972).

In this paper we investigate the influence of SST anomalies over the South Atlantic on the atmospheric circulation. Due to asymmetries in continental geometry, the “meteorological equator,” defined by the meridional position of the ITCZ lies generally north of the equator. The eastern equatorial cold tongue—where El Niño-like dynamics is believed to operate—is open to the South Atlantic but isolated from the North Atlantic by West Africa. The subtropical anticyclone over the South Atlantic directly influences the equatorial eastern Atlantic through the SE Trade winds. Thus, it is likely that variations in the subtropical high can influence the equatorial mode. There is a good deal of similarity with the eastern equatorial Pacific in this respect.

An additional factor motivating the potential importance of the South Atlantic in tropical Atlantic climate variability is the presence of the summer monsoonal circulation over South America (Horel et al. 1989). The Amazonian convergence zone that develops in austral summer and extends southeastward to form the South Atlantic Convergence Zone (SACZ) is intimately related to the strength and position of the subtropical anticyclone over the South Atlantic. The relationship is established both through the compensation of ascent and descent in thermodynamically direct overturning cells (Gandu and Silva Dias 1998), as well as through the southward advection of moist static

energy into the subtropical convergence zone over South America on the western flank of the subtropical anticyclone (Kodama 1992, 1993). The narrowness of the tropical Atlantic Ocean compared to the Pacific makes the adjacent land-based convection zones of potential importance to the atmospheric circulation over the ocean and, in particular, to the terrestrial extensions of the ITCZ into equatorial Africa and NE Brazil.

Interannual variations in the strength and position of the subtropical anticyclone are accompanied by SST anomalies over the subtropical South Atlantic (Venegas et al. 1997), as are interannual changes in the intensity of the SACZ (Robertson and Mechoso 2000; Barros et al. 2000). Several studies suggest that subtropical SST anomalies over the South Atlantic are largely due to local thermodynamic forcing by the atmosphere (Kalnay et al. 1986, Venegas et al. 1997, Sterl and Hazeleger 2002). However, the SACZ-related SST anomalies are dipolar with a nodal line running approximately along the confluence between the Brazil and Malvinas currents off southeastern South America, which suggests a potential role of oceanic advection in the establishment of this feature.

The relationship between the tropical and subtropical Atlantic can only be understood by considering the seasonal cycle. The SACZ and South American monsoon system (SAMS) reach their peak intensities in December–March, which is the season when SST anomalies over the subtropical South Atlantic are most intense. In April, with convection over land retreating rapidly northward, the ITCZ reaches its *southernmost* position over Northeast Brazil. Starting in May–June, SST variability over the South Atlantic becomes dominated by the equatorial cold-tongue complex, with subtropical variability greatly diminished.

This paper presents simulations with an atmospheric general circulation model (GCM) designed to investigate the sensitivity of the atmosphere to South Atlantic SST anomalies during the calendar half-year January–June, focusing on subtropical SACZ-related anomalies in January–March, and the increasingly strong equatorial anomalies that develop by June. We present and validate the hypothesis that events over the subtropical South Atlantic during January–March can influence the equatorial eastern Atlantic SST in April–June where the atmosphere is sensitive to them, and the implications for seasonal predictability.

Section 2 describes the GCM experiments. The SACZ-related SST anomaly experiment is presented in Sect. 3. In Sect. 4, we derive the seasonally varying SST anomaly forcing and describe the GCM’s response to it. Section 5 contains a discussion and conclusions.

2. Model and simulations

We use the UCLA AGCM, which includes advanced parameterizations of the major physical processes in the atmosphere. The parameterization of cumulus convection is a version of the Arakawa-Schubert scheme (Arakawa and Schubert 1974) in which the cloud work function quasi-equilibrium assumption is relaxed by predicting the cloud-scale kinetic energy (Randall and Pan 1993). PBL processes are parameterized using the mixed-layer approach of Suarez et al. (1983) as recently revised by Li and Arakawa (1999); these modifications result in much improved surface latent heat fluxes and stratocumulus cloud incidence. The parameterization of radiative processes is from

Harshvardhan et al. (1987, 1989). A more detailed description of the model can be found in Mechoso et al. (2000) and electronically at <http://www.atmos.ucla.edu/esm/agcmdir>.

The work is performed with the high resolution 2.5° longitude by 2° latitude, 29 layer configuration of the model version (6.98), which is identical to that used by Farrara et al. (2000) in their study of the atmospheric response to the 1997–8 El Niño. The integrations cover the period November 1–March 31 (Sect. 3) and November 1–September 30 (Sect. 4). The initial conditions were obtained by adding small random perturbations to the model's prognostic variables corresponding to an atmospheric state in northern fall (October 1). Two ten-member control ensembles were performed using GISST climatological SSTs 1960–1990 (Rayner et al. 1995). Two additional ensembles were performed, each with different distributions of SST anomalies added to the climatological fields, as described in Sects. 3 and 4 below.

3. Subtropical cold anomaly

Figure 1 shows the leading empirical orthogonal function (EOF) of interannual atmospheric circulation variability over subtropical South America in summer (January–March, hereafter JFM), as constructed from the NCAR-NCEP Reanalysis data (Kalnay et al. 1996) by Robertson and Mechoso (2000). Panel (a) consists of regression maps with 850-hPa winds and 500-hPa omega vertical velocity, and shows an intensified SACZ accompanied by anomalous descent to the southwest, and by a cyclonic wind field such that anomalous ascent coincides with anomalous northwesterly winds and vice versa. Thus, tropical moisture is channeled into the SACZ, while the opposite occurs to the southwest (the low-level southward jet east of the Andes (Ref) is weakened, resulting

in less advection of moisture-rich air into SE South America). Panel (b) shows the analogous regression map of GISST SST, with broad-scale subtropical cold anomalies and weak warm anomalies to the south.

The SST anomaly distribution in Fig. 1b was multiplied by a factor of three to enhance the signal-to-noise ratio, yielding maximum cold anomalies of about 1K, and prescribed as a fixed SST anomaly on top of the monthly GISST climatology in an ensemble of 9 November–March simulations. Figure 2 shows the GCM’s JFM-average response, with the statistically significant areas (shaded at 95%) computed using a two-sided Student t-test with one degree of freedom per simulation (minus 1), giving 28 in all (using both 10-member control runs to compare against). The response is not significant either in the upper troposphere or outside the geographical domain shown.

The GCM’s response shows a broad, local, cold lower-tropospheric anomaly with net-heat flux anomalies into the ocean, tending to damp the prescribed cold SST anomaly. Rainfall is reduced over the cold anomaly, with both precipitation and temperature anomalies that are strongest over the ocean and extend northwestward over the continent. The anomalous wind and omega fields exhibit the same relationship to each other as seen in the observed anomalies in Fig. 1. What is obvious, however, is that the polarity of the simulated anomalies is the opposite of the observed ones. As discussed in Sect. 5, the implication is that the SST anomalies in Fig. 1b are forced by the atmosphere, confirming previous ideas, e.g. Kalnay et al. (1986). The nodal line of the precipitation anomalies roughly coincides with the axis of the GCM’s climatological SACZ, so that the anomalies tend to be associated with shifts in the SACZ.

4. Evolving basin-scale pattern

To take a broader perspective of South Atlantic SST anomalies, Fig. 3 shows the leading EOF of seasonal-mean SST variability for the January–March (JFM) and April–June (AMJ) seasons over the South Atlantic, 0–30°S. These were computed from the Reynolds and Smith (1994) extended SST dataset 1950–1999, with the linear trend subtracted. In both seasons, the leading EOF has the same polarity covering the tropics and subtropics, with maxima in the equatorial cold-tongue region as well as in the subtropics near 20°S. The dominant region of variability, however, clearly shifts from the subtropics in JFM to the equatorial cold-tongue and Gulf of Guinea in AMJ. In the second half of the calendar year (not shown), the AMJ pattern persists while weakening.

Figure 4 shows a sequence of SST patterns derived from the leading principal component (PC) of *monthly* SST variability (0–30°S), with the mean seasonal cycle and linear trend subtracted. Each panel in Fig. 4 was derived by regressing the monthly PC onto the set of SST maps restricted to each respective calendar month. The amplitudes have been scaled by a factor of two, yielding a positive anomaly maxima of about 1K. The resulting sequence captures the seasonal evolution in pattern seen in Fig. 3, and is used to force the GCM. The SST anomaly distributions shown in Fig. 4 were added to the GISST climatology used in Sect. 3, interpolating linearly in time, and an ensemble of 10 November–September simulations made. It was verified that the GISST and Reynolds climatologies for each calendar month are almost identical.

Figures 5 and 6 show the GCM’s seasonally averaged response in JFM and AMJ respectively, compared to a ten-member ensemble with climatological time-varying

SSTs. During JFM (Fig. 5) the subtropical response is broadly similar to that seen in Fig.2, albeit with reversed polarities. The lower troposphere warms throughout the subtropics and tropics; subtropical amplitudes (at 850 hPa) closely reflect the prescribed anomaly. There is a response in the model's SACZ, but it is much weaker than the one in Sect. 3, probably because the SST EOF patterns in Fig. 4 do not extend to the South American coast. The dynamical response is clearly strongest in the equatorial region, despite the relatively weak local anomalies. The simulated equatorial response shows the hallmarks of the classical Matsuno (1966) - Gill (1980) response to a deep atmospheric heat source at the equator, with strong low-level westerlies to the west of the heat source.

The net surface heat flux is directed strongly into the atmosphere in the equatorial cold-tongue region, as expected from the warm anomaly there. More surprising are the strong anomalous fluxes directed into the ocean to the south, even though SST anomalies are weakly positive there. The heat flux anomalies over the subtropics are more complex than those seen in Sect. 3.

In April–June, the SST anomalies in Fig. 4 strengthen in the equatorial cold-tongue and weaken in the subtropics. The GCM's dynamical response in that season becomes strongly confined to the equator with large rainfall anomalies throughout the Atlantic accompanied by strong low-level westerly anomalies. The GCM remains sensitive to the subtropical SST anomalies in low-level temperature, and these spread eastward into most of Africa. Net surface heat flux anomalies are only statistically significant in the equatorial cold tongue region, where they act to damp the SST anomaly. This is the typical situation over the equatorial Pacific during ENSO.

The global response during AMJ is shown in Fig. 7 in terms of 200-hPa wind, streamfunction, and precipitation. The precipitation anomalies in the tropical Atlantic sector are largely confined to ocean areas, with a remote negative anomaly over the western Indian Ocean. The only significant land feature is a band of weak positive anomalies over sub-Saharan Africa. Anticyclones occur at upper levels on either side of the equator. However, in contrast to the Pacific case during El Niño episodes, there is a noticeable meridional tilt with the anticyclone to the north being displaced eastward over Africa. The GCM results also indicate significant Rossby wave propagation northeastward into Europe and southwestward to southern South America. Thus, there is a marked meridional asymmetry not seen over the Pacific during ENSO.

5. Discussion and conclusions

Our goal in this paper is to illuminate outstanding aspects of ocean-atmosphere interactions over the South Atlantic by examining the response of an atmospheric GCM to oceanic anomalies prescribed in the tropics and subtropics. In a previous study of atmospheric variability over South America based on an EOF analysis of winds from observational data, Robertson and Mechoso (2000) found that interannual changes in the intensity of the SACZ during austral summer are associated with simultaneous SST anomalies over the SW Atlantic. Here we show that this type of SST anomaly prescribed in the boundary conditions of our GCM does significantly influence the simulated SACZ and associated low-level wind anomalies. The influence, however, is of the opposite sense to the one observed: while an intensified SACZ is observed to be predominantly

accompanied by cold SST anomalies around 10–30°S (Fig. 1), prescribing the latter acts to *damp* the GCM's SACZ and to displace it poleward.

In spite of the opposition of signs, the GCM response does capture the dipole-type structure of the vertical motion anomalies associated with interannual variability of the SACZ, as well as the associated low-level eddy circulation (Figs. 1a and 2a). Thus, anomalous ascent in the simulation is accompanied by anomalous northwesterlies, and vice versa. On the other hand, the observed SACZ circulation anomalies documented in Robertson and Mechoso (2000) are highly coherent in the upper troposphere while the GCM response reported here is not. The vorticity balance of the observed upper-tropospheric vortex bears the hallmark of a stationary Rossby wave that can be excited opportunistically through wave dispersion from the Pacific. This may take place on sub-monthly time scales through synoptic-scale waves (Liebmann et al. 1999), 40–60-day tropical intraseasonal oscillations (Nogués-Paegle and Mo 1997, Paegle et al. 2000), and is seen also seen during ENSO episodes (Cazes et al. 2002). The GCM fields resemble the local response to surface thermal forcing. One should be cautious in interpreting the lack of vertical coherence in the simulation as either supporting or challenging a physical hypothesis, however, since the control run of the GCM does not entirely succeed in capturing that feature.

Barreiro et al. (2002) have examined the response of the SACZ to Atlantic SST anomalies using an ensemble of long simulations with the CCM3 GCM, forced by observed SSTs. Our results are quite similar to their leading SST-forced mode in terms of the anomalous low-level winds and precipitation. The atmospheric response is more

confined to the ocean in their case, consistent with their associated SST anomaly being centered further east.

Venegas et al. (1997) have studied the covariability between SST and sea-level pressure (SLP) over the South Atlantic from COADS data. Their first mode of covariability consists of an SST distribution that is rather similar to Fig. 1b. The accompanying distribution of SLP anomalies reflects changes in strength of the subtropical anticyclone, such that an intensified anticyclone goes together with colder subtropical SSTs. The mode is strongest in austral summer, consistent with the seasonal cycle of SST variability (Fig. 4). The covariability is largest when SLP leads SST by 1-2 months, suggestive of an atmosphere-to-ocean forcing. Figure 8 shows lag-correlation maps of Reynolds SST, constructed from the observed interannual PC used in Fig. 1. There is a clear indication that SST anomalies off the Brazilian coast do tend to lag the SACZ, rather than precede it. Figs. 8b and c suggest that there may also be a link with the Pacific off the coast of Chile. The latter feature was not seen contemporaneously in the GISSST data set. While the GCM results in Sect. 3 indicate that SST anomalies over the SW Atlantic play a secondary role, the SST lag correlations in Fig. 8c suggest that SST anomalies generated by the SACZ during austral summer (JFM) may persist into austral fall (AMJ) when they have the potential to influence the climate of southeastern South America (Diaz et al 1998).

Interannual variability of the SACZ is complex because it is influenced by Rossby-wave propagation from the Pacific, the subtropical anticyclone over the South Atlantic as well as SST anomalies there. It has also been suggested that the North Atlantic Oscillation can play a role (Robertson and Mechoso 1998).

The dominant seasonal variation in SST anomalies over the South Atlantic appears as a “migration” between the subtropics in austral summer and the equatorial cold-tongue complex in austral fall (Figs. 3 and 4). It is not apparent whether this migration constitutes a true physical connection between the subtropics and equatorial regions, such that anomalies in the former during JFM might be precursors of others in the latter during AMJ. Mo and Häkkinen (2001) have proposed a linkage between El Niño and the tropical Atlantic, by way of a wave train extending from the Pacific into the South Atlantic.

The strong deep dynamical character of the tropical response in AMJ (Fig. 6 and 7) is striking, compared to the mostly local thermodynamical extratropical response in JFM (Fig. 5). The equatorial response in AMJ consists of a near-zonal band of pronounced rainfall anomalies that extend across the entire equatorial Atlantic, with a clear southward tilt toward NE Brazil. Rainfall anomalies are largely confined to oceanic areas with compensating dry regions over the tropical North Atlantic and Indian Ocean. The only noticeable anomaly over land is over sub-Saharan Africa. This particular anomaly is most pronounced during June, and less so in July–September (not shown). While the anomaly is confined to a single month in the simulation, it is nonetheless statistically significant and could be interpreted as an early onset to the wet season there. It is somewhat surprising that the precipitation anomalies do not extend more into the continents although the mean seasonal cycle of precipitation is simulated quite realistically. One potentially limiting factor in this regard is that the GCM does not include interactive land surface processes. Barreiro et al. (2002) report a similar finding in the CCM3 model.

The remote extratropical response of the atmosphere to the equatorial Atlantic SST anomalies is strongest in May, and yields significant 200-hPa wind anomalies extending from southern South America to Europe in the AMJ seasonal mean; there is considerable inter-hemispheric asymmetry, in contrast to the rather symmetric extratropical response to El Niño during boreal winter.

The interannual SST anomalies over the subtropical South Atlantic and the equatorial cold tongue are highly correlated, as demonstrated in Fig. 9. (The correlation between the two regions is highest in March (0.66) and lowest in July (0.36)). A plausible physical explanation is that variations in the strength and position of the subtropical anticyclone are affected by the SST distribution in the austral summer, at which time the leading EOF of SLP interannual variability reaches closest to the equator, near 35°S (while the axis of the subtropical high is near 30°S). It is conceivable that Bjerknes-type coupled ocean-atmosphere interactions in the equatorial cold tongue (i.e. the “equatorial mode”) in the boreal summer can amplify SST anomalies originated over the South Atlantic during the previous boreal spring. Since the former strongly impact the atmosphere, this chain of events deserves attention as a potentially important source of seasonal predictability. Interannual SST anomalies in the tropical North Atlantic are also large during boreal spring. These may also impact the equatorial mode, leading to small predictability from any one source alone.

Acknowledgments: We are grateful to Ping Chang and Marcelo Barreiro for useful discussions. This work was supported primarily by NOAA grant NA06GPO427 under the CLIVAR-Atlantic program, and by NOAA under grant NA06GP0511. The NCEP-

NCAR reanalysis data were provided through the NOAA Climate Diagnostics Center (<http://www.cdc.noaa.gov/>).

References

- Arakawa, A., and W. H. Schubert, 1974: Interaction of a cumulus ensemble with the large-scale environment, Part I. *J. Atmos. Sci.*, **31**, 674-701.
- Barreiro, M., P. Chang, and R. Saravanan, 2002: Variability of the South Atlantic Convergence zone simulated by an atmospheric general circulation model. *J. Climate*, **15**, 745-763.
- Barros V., M. Gonzalez, B. Liebmann, and I. Camilloni, 2000: Influence of the South Atlantic convergence zone and South Atlantic Sea surface temperature on interannual summer rainfall variability in Southeastern South America. *Theor. Appl. Climatol.*, **67**, 123-133.
- Cazes, G., A. W. Robertson, and C. R. Mechoso, 2002: Seasonal dependence of teleconnections over South America. *J. Climate*, sub judice.
- Chang, P., L. Ji, and H. Li, 1997: A decadal climate variation in the tropical Atlantic ocean from thermodynamic air-sea interactions. *Nature*, **385**, 516-518.
- Chang, P., R. Saravanan, L. Ji, and G. C. Hegerl, 2000: The effect of local sea-surface temperatures on atmospheric circulation over the tropical Atlantic sector. *J. Climate*, **13**, 2195-2216.

- Davis, R. E., 1976: Predictability of sea surface temperature and sealevel pressure over the North Pacific. *J. Phys. Oceanogr.*, **6**, 249-266.
- Diaz, A. F., C. D. Studzinski, and C. R. Mechoso, 1998: Relationships between precipitation anomalies in Uruguay and Southern Brazil and sea surface temperatures in the Pacific and Atlantic oceans. *J. Climate*, **11**, 251-271.
- Dommenget, D., and M. Latif, 2000: Interannual to decadal variability in the tropical Atlantic. *J. Climate*, **13**, 777-792.
- Enfield, D.B., and D.A. Mayer, 1997: Tropical Atlantic sea surface temperature variability and its relation to El Niño-Southern Oscillation. *J. Geophys. Res.*, **102**, 929-945.
- Farrara, J. D., C. R. Mechoso, and A. W. Robertson, 2000: Ensembles of AGCM two-tier predictions and simulations of the circulation anomalies during winter 1997-98. *Mon. Wea. Rev.*, **128**, 3589-3604.
- Folland, C., Owen, J., Ward, M. N., Colman, A. 1991. Prediction of seasonal rainfall in the Sahel region using empirical and dynamical methods. *J. Forecasting*, **10**, 21-56.
- Gill, A. E., 1980: Some simple solutions for heat-induced tropical circulation. *Quart. J. Roy. Meteor. Soc.*, **106**, 447-462.
- Gandu, A. W., Silva Dias, P. L. 1998: Impact of tropical heat sources on the South American tropospheric upper circulation and subsidence *J. Geophys. Res.* **103** , 6001-6015.

- Harshvardhan, R. Davies, D. A. Randall and T. G. Corsetti, 1987: A fast radiation parameterization for atmospheric circulation models. *J. Geophys. Res.*, **92**, 1009-1016.
- Harshvardhan, D. A. Randall, T. G. Corsetti, and D. A. Dazlich, 1989: Earth radiation budget and cloudiness simulations with a general circulation model. *J. Atmos. Sci.* **46**, 1922-1942.
- Hastenrath, S., and L. Heller, 1977: Dynamics of climate hazards in Northeast Brazil. *Quart. J. Roy. Meteor. Soc.*, **103**, 77-92.
- Horel, J. D., A. N. Hahnmann, and J. E. Geisler, 1989: An investigation of the annual cycle of the convective activity over the tropical Americas. *J. Climate*, **2**, 1388-1403.
- Kalnay, E., K. C. Mo and J. Paegle, 1986: Large-amplitude, short-scale stationary Rossby waves in the Southern Hemisphere: Observations and mechanistic experiments to determine their origin. *J. Atmos. Sci.*, **43**, 252-275.
- Kalnay, E., M. Kanamitsu, R. Kistler, W. Collins, D. Deaven, L. Gandin, M. Iredell, S. Saha, G. White, J. Woollen, Y. Zhu, M. Chelliah, W. Ebisuzaki, W. Higgins, J. Janowiak, K. C. Mo, C. Ropelewski, J. Wang, A. Leetmaa, R. Reynolds, R. Jenne, and D. Joseph, 1996: The NCEP/NCAR 40-year Reanalysis project. *Bull. Amer. Meteor. Soc.*, **77**, 437-470.
- Kodama, Y.-M., 1992: Large-scale common features of subtropical precipitation zones (the Baiu frontal zone, the SPCZ, the SACZ) Part I: Characteristics of subtropical frontal zones. *J. Meteor. Soc. Japan*, **70**, 813-835.

- Kodama, Y.-M., 1993: Large-scale common features of subtropical precipitation zones (the Baiu frontal zone, the SPCZ, the SACZ) Part II: Conditions of the circulations for generating the STCZs. *J. Meteor. Soc. Japan*, **71**, 581-610.
- Lamb, P. J., 1978a: large scale tropical Atlantic surface circulation patterns associated with sub-Saharan weather anomalies. *Tellus*, **30**, 240-251.
- Lamb, P. J., 1978b: Case studies of tropical Atlantic surface temperatures and rainfall during recent sub-Saharan weather anomalies: 1967 and 1968. *Mon. Wea. Rev.*, **106**, 482-491.
- Li, J.-L. and A. Arakawa, 1999: Improved simulation of PBL moist processes with the UCLA GCM. Preprints, *Seventh Conf. On Climate Variations*, Long Beach, CA, Amer. Meteor. Soc., 35-40.
- Liebmann, B., G. N. Kiladis, J. A. Marengo, T. Ambrizzi, and J. D. Glick, 1999: Submonthly convective variability over South America and the South Atlantic Convergence Zone. *J. Climate*, **12**, 1877-1891.
- Matsuno, T., 1966: Quasi-geostrophic motions in the equatorial area. *J. Meteor. Soc. Japan, Ser. II*, **44**, 25-43.
- Mechoso, C. R., J.-Y. Yu and A. Arakawa, 2000: A coupled GCM pilgrimage: From climate catastrophe to ENSO simulations. *General circulation model development: Past, present and future. Proceedings of a Symposium in Honor of Professor Akio Arakawa*, D. A. Randall, Ed., Academic Press, pp. 539-575.
- Mo, K. C., and S. Häkkinen, 2001: Interannual variability in the tropical Atlantic and linkages to the Pacific. *J. Climate*, **14**, 2740-2762.

- Moura, A. D., and J. Shukla, 1981: On the dynamics of droughts in Northeast Brazil: observations, theory and numerical experiments with a general circulation model. *J. Atmos. Sci.*, **38**, 2653-2675.
- Namias, J., 1972: Influence of northern hemisphere general circulation on drought in northeastern Brazil. *Tellus*, **24**, 336-342.
- Nogués- Paegle, J., and K.C. Mo, 1997: Alternating wet and dry conditions over South America during summer. *Mon. Wea. Rev.*, **125**, 279-291.
- Paegle, J. N., L. A. Byerle, and K. C. Mo, 2000: Intraseasonal modulation of South American summer precipitation. *Mon. Wea. Rev.*, **128**, 837-850.
- Randall, D. A., and D. M. Pan, 1993: Implementation of the Arakawa-Schubert cumulus parameterization with a prognostic closure. *The representation of cumulus convection in numerical models of the atmosphere*, K. A. Emanuel and D. J. Raymond, Ed., American Meteorological Society, 137-144.
- Rayner, N. A., C. K. Folland, D. E. Parker, and E. B. Horton, 1995: A new global sea-ice and sea surface temperature (GISST) data set for 1903-1994 for forcing climate models. Hadley Centre Internal Note No. 69, pp. 13.
- Reynolds, R. W., and T. M. Smith, 1994: Improved global sea surface temperature analyses using optimum interpolation. *J. Climate*, **7**, 929-948.
- Robertson, A. W., and C. R. Mechoso, 1998: Interannual and decadal cycles in river flows of southeastern South America. *J. Climate*, **11**, 2570-2581.
- Robertson, A. W., and C. R. Mechoso, 2000: Interannual and interdecadal variability of the South Atlantic convergence zone. *Mon. Wea. Rev.*, **128**, 2947-2957.

- Saravanan, R., and P. Chang, 2000: Interactions between tropical Atlantic variability and El Niño-Southern Oscillation. *J. Climate*, **13**, 2177-2194.
- Sterl, A., and W. Hazeleger, 2002: Patterns and mechanisms of air-sea interaction in the South Atlantic Ocean. *J. Climate*, submitted.
- Suarez, M. J., A. Arakawa and D. A. Randall, 1983: The parameterization of the planetary boundary layer in the UCLA general circulation model: Formulation and results. *Mon. Wea. Rev.*, **111**, 2224-2243.
- Tseng, L., and C. R. Mechoso, 2000: A quasi-biennial oscillation in the equatorial Atlantic Ocean. *Geophys. Res. Lett.*, **28**, 187-190.
- Venegas, S.A., L.A. Mysak, and D.N. Straub, 1997: Atmosphere-ocean coupled variability in the South Atlantic. *J. Climate*, **10**, 2904-2920.
- Zebiak, S. E., 1993: Air-sea interaction in the equatorial Atlantic region. *J. Climate*, **6**, 1567-1586.

Figure Captions

Figure 1: Regression maps of the leading PC of 200-hPa JFM-averaged winds 1958–97 over southern South America from the NCEP-NCAR Reanalysis. (a) 850-hPa winds and 500-hPa omega, (b) GISST SST. In (a), only vectors whose correlations with the PC are significant at the 95% level are plotted, with the number of degrees of freedom of the two-sided Student *t*-test estimated at each grid point from the decorrelation times of the PC and winds time series (Davis 1976). See Robertson and Mechoso (2000) for further details. Contour intervals are (a) $0.2 \times 10^{-2} \text{ Pa s}^{-1}$, and (b) 0.05 K, with zero contour omitted.

Figure 2: January–March average GCM response to the SST anomaly pattern in Fig. 1b, with the latter scaled by a factor of three. (a) 850-hPa winds and 500-hPa omega (contours), (b) 850-hPa temperature, (c) precipitation, and (d) net surface heat flux into the atmosphere. The response is defined as the difference between an ensemble of 9 anomaly simulations and 20 control simulations (see text). Shading indicates the 95% significance level, computed from a two-sided Student *t*-test with 28 degrees of freedom, while in panel (a) only similarly significant vectors are plotted. Contour intervals are (a) $0.5 \times 10^{-2} \text{ Pa s}^{-1}$, (b) 0.2 K, (c) 0.2 mm day^{-1} , and (d) 5 W m^{-2} ; zero contours are omitted. Panels (c) and (d) are spatially smoothed with a 5-point-average smoother.

Figure 3: The leading seasonal-mean EOFs of the (linearly detrended) Reynolds SST data set 1950–99, computed over the South Atlantic 0° – 30° S for (a) January–March, and (b) April–June. Shown are regression maps with the respective PC. Contour interval is 0.1 K, with the zero contour omitted.

Figure 4: Season evolution of SST anomalies used to force the GCM in the experiment described in Sect. 4. See text for details. Contour interval is 0.2 K, with the zero contour omitted.

Figure 5: January–March average GCM response to the SST anomaly evolution in Fig. 4. (a) 850-hPa winds and 500-hPa omega (contours), (b) 850-hPa temperature, (c) precipitation, and (d) net surface heat flux into the atmosphere. The response is defined as the difference between an ensemble of 10 anomaly simulations and 10 control simulations (see text). Shading indicates the 95% significance level, computed from a two-sided Student t -test with 19 degrees of freedom, while in panel (a) only similarly significant vectors are plotted. Contour intervals are (a) $0.5 \times 10^{-2} \text{ Pa s}^{-1}$, (b) 0.2 K, (c) 0.5 mm day^{-1} , and (d) 5 W m^{-2} ; zero contours are omitted. Panels (c) and (d) are spatially smoothed with a 5-point-average smoother.

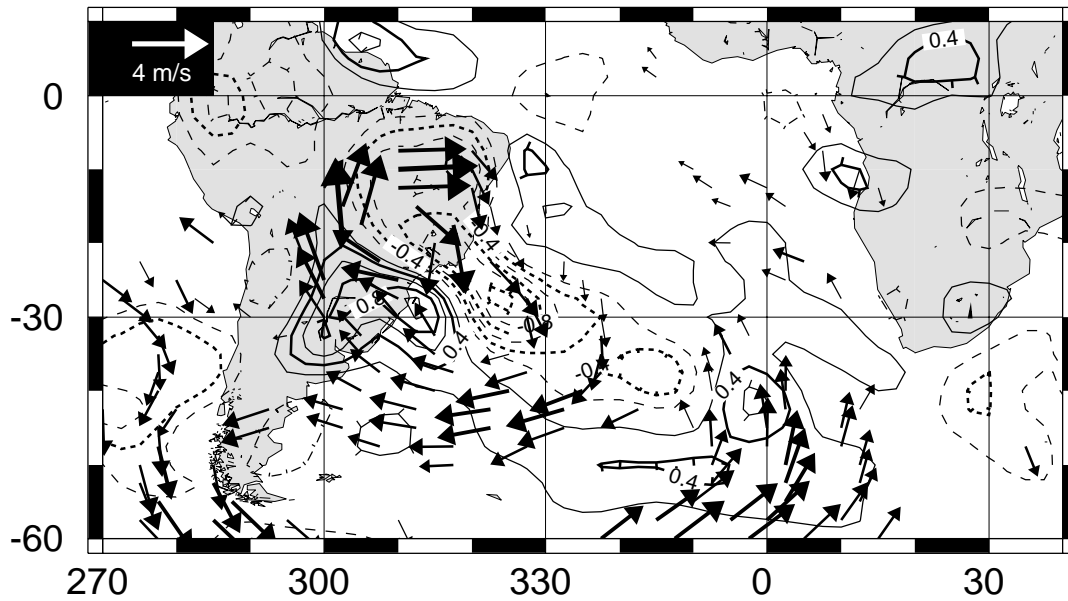
Figure 6: April–June average GCM response to the SST anomaly evolution in Fig. 4. Details as in Fig. 5.

Figure 7: Global April–June response to the SST anomaly evolution in Fig. 4. (a) 200-hPa winds and streamfunction (contour interval $1.5 \times 10^{-6} \text{ m}^2 \text{ s}^{-1}$, zero contour included), (b) precipitation. Details as in Fig. 5.

Figure 8: Correlation maps of seasonal mean Reynolds SST with the January–March PC used to construct Fig. 1. (a) preceding October–February, (b) contemporaneous January–March, and (c) the following April–June. Locally 95% significant areas are shaded, as in Fig. 1. Contour interval is 0.1, with zero contour omitted.

Figure 9: Annual-mean anomaly time series of Reynolds SST averaged over boxes in the eastern equatorial Atlantic (2°N – 4°S , 10°W – 0°E ; solid line), and the subtropical South Atlantic (14°S – 26°S , 20°W – 0°E ; dashed line).

a) uv850/om500



b) SST

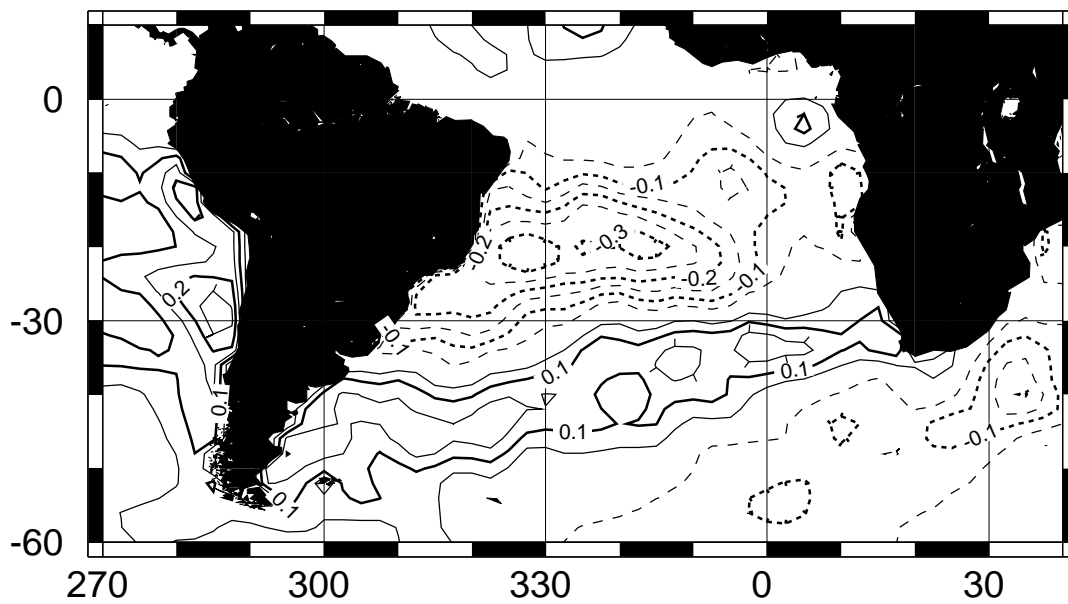
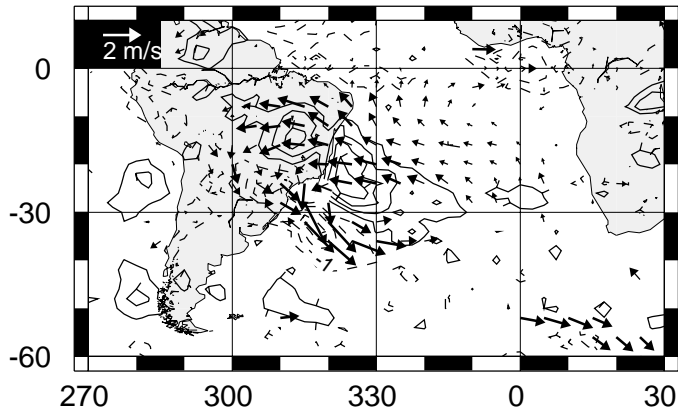
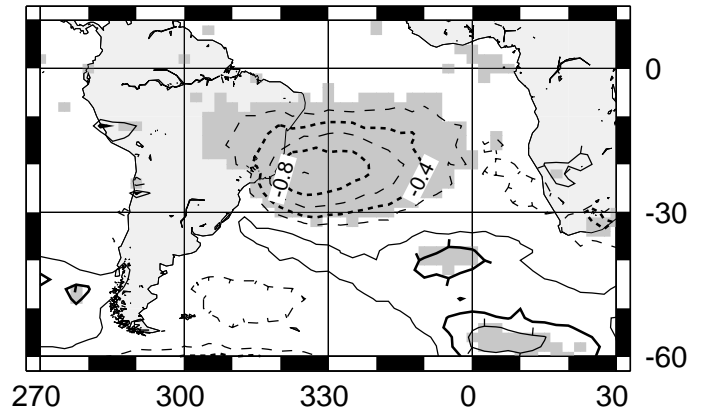


Figure 1

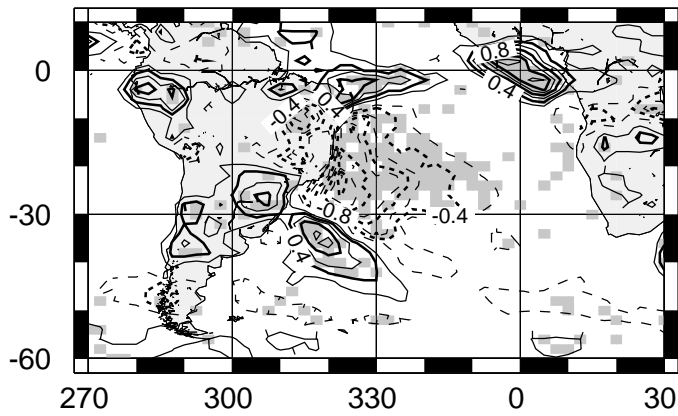
a) uv850/om500



b) T850



c) Precipitation



d) Net Sfc Heat Flux Up

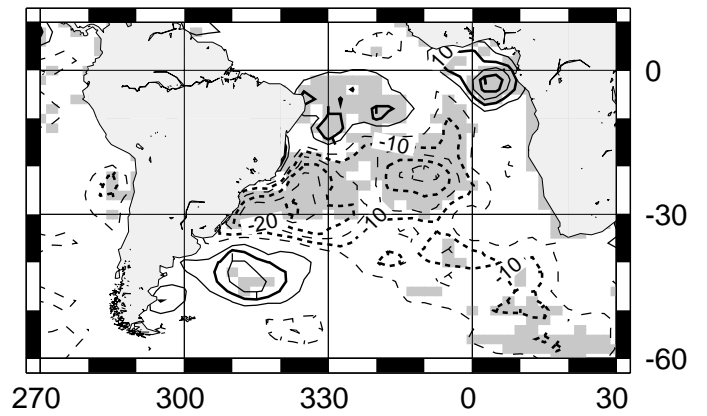
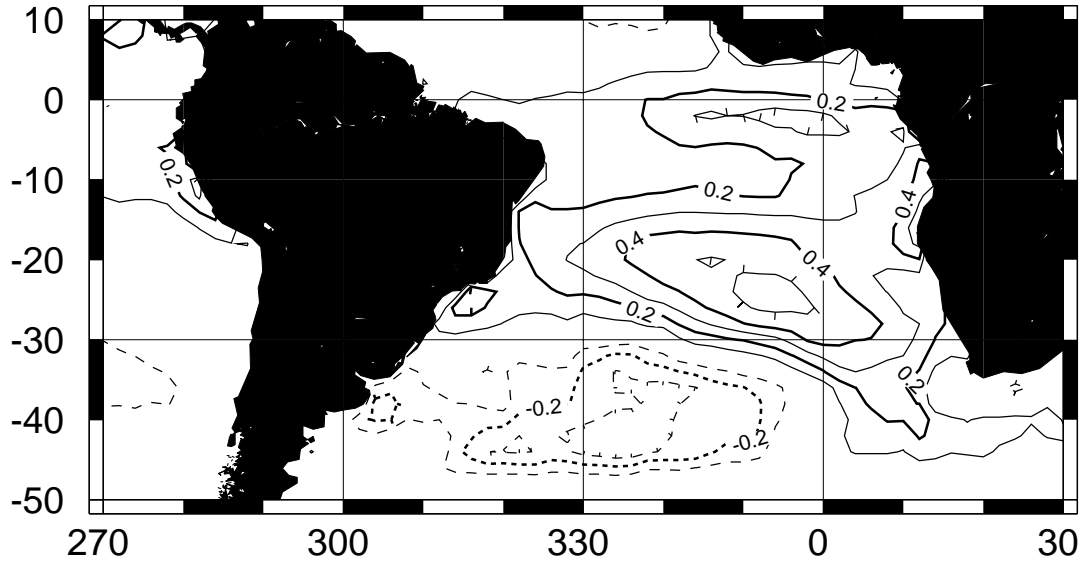


Figure 2

a) EOF 1 January-March (56.1%)



b) EOF 1 April-June (54.6%)

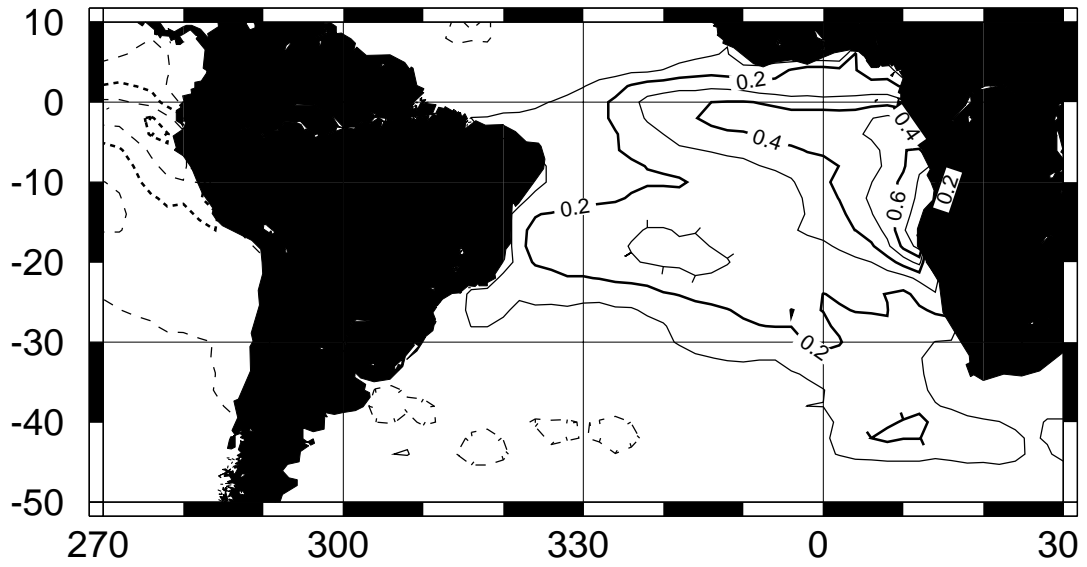


Figure 3

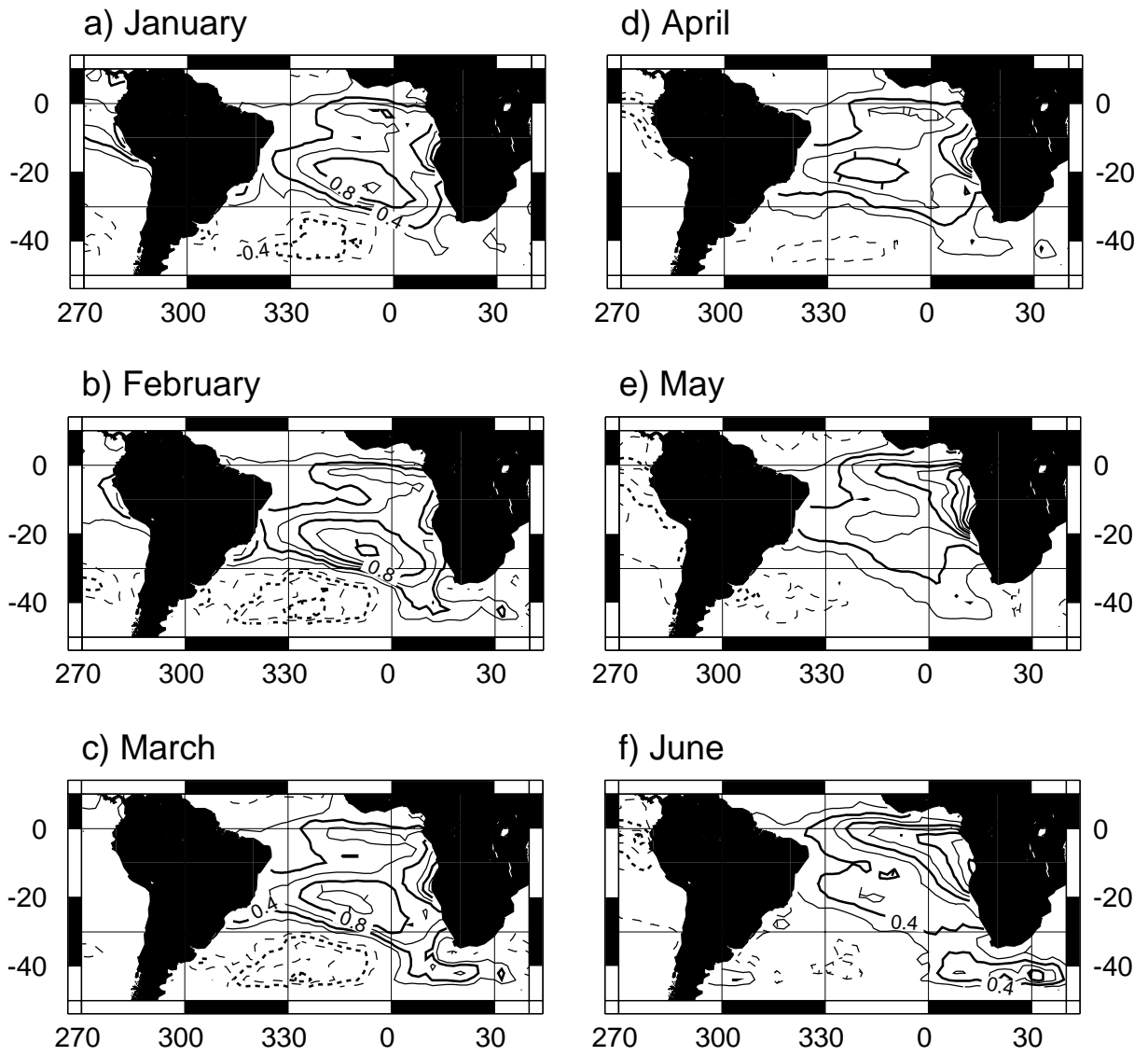
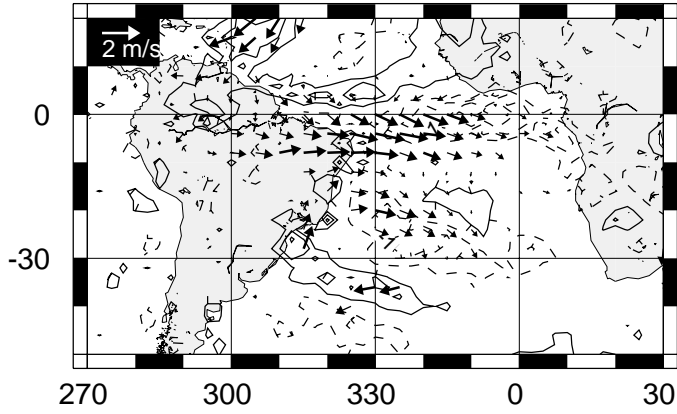
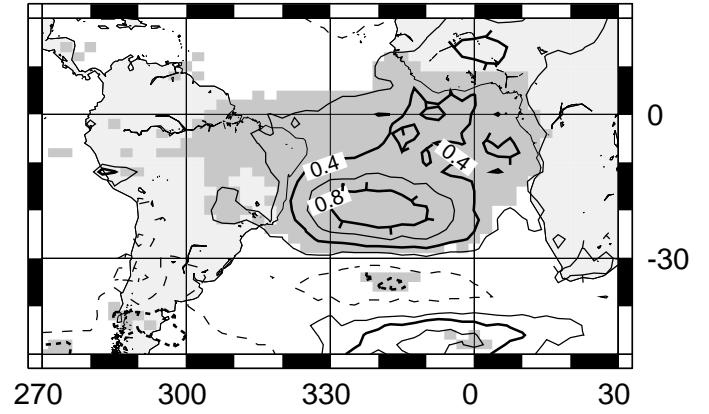


Figure 4

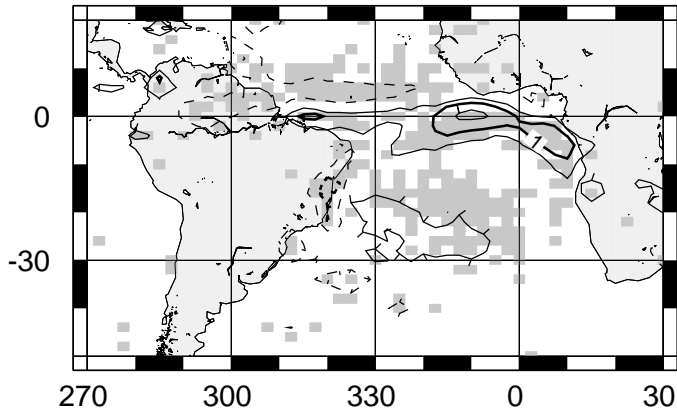
a) uv850/om500



b) T850



c) Precipitation



d) Net Sfc Heat Flux Up

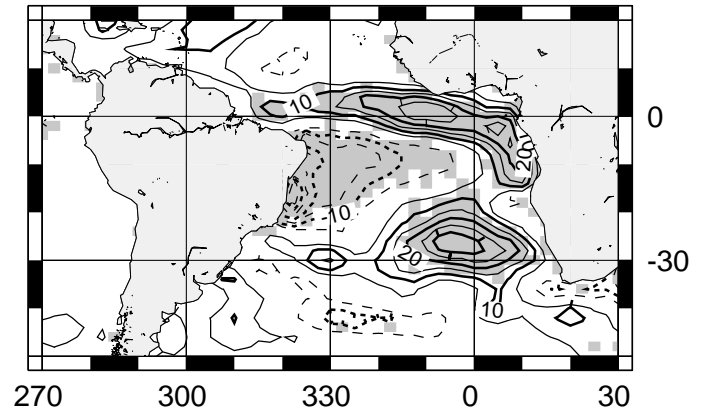
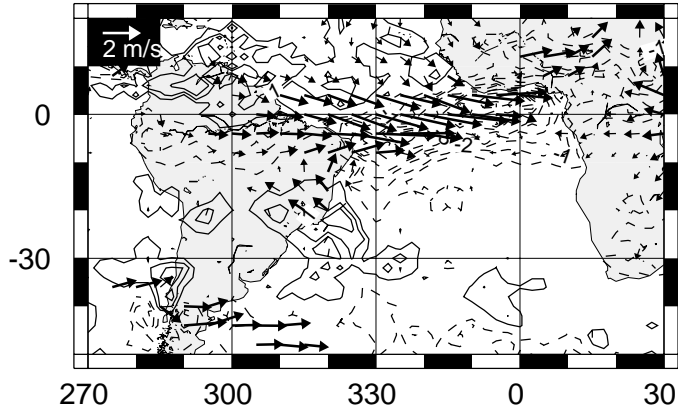
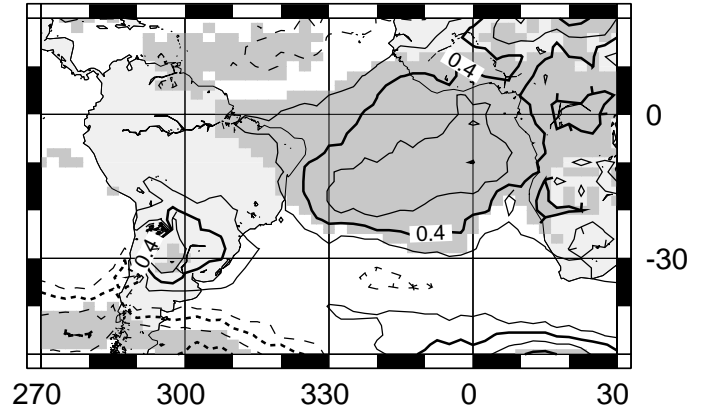


Figure 5

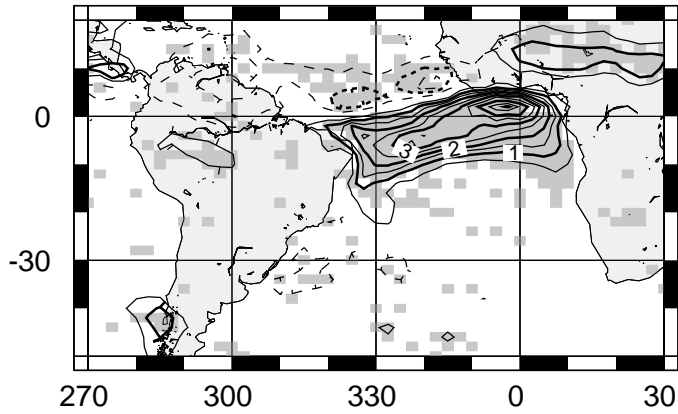
a) uv850/om500



b) T850



c) Precipitation



d) Net Sfc Heat Flux Up

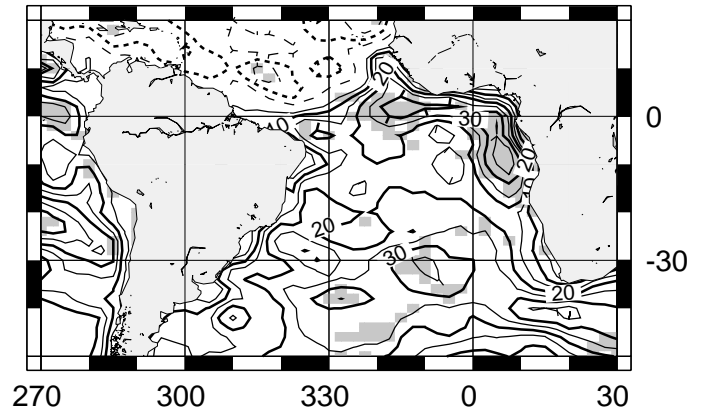
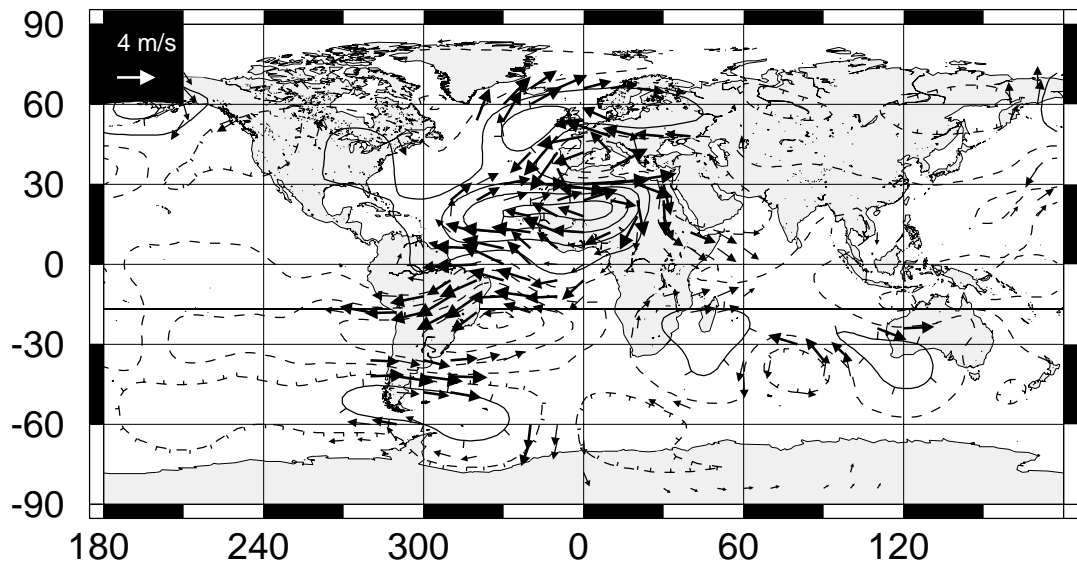


Figure 6

a) uv & psi200



b) Precipitation

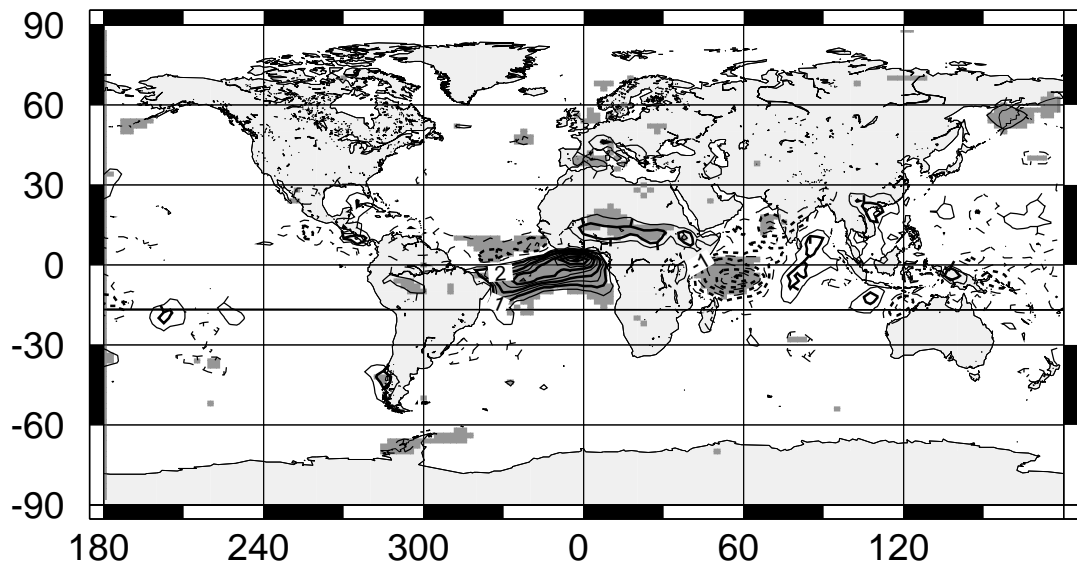
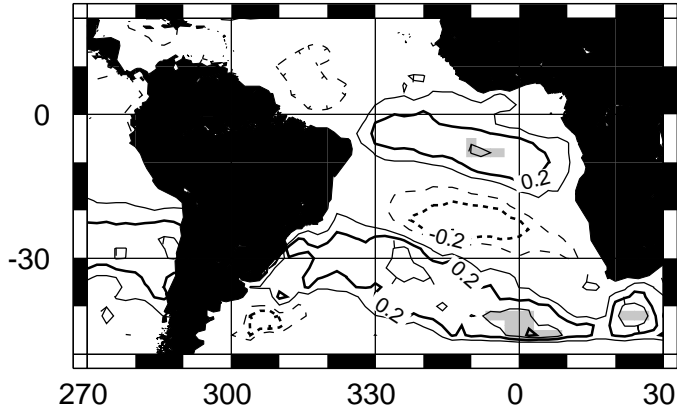
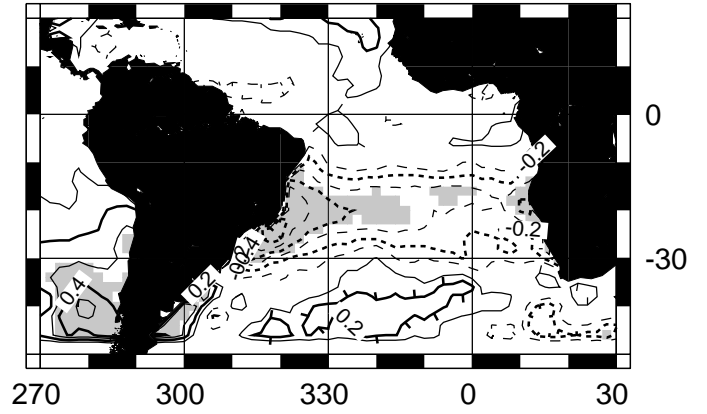


Figure 7

a) October-December



b) January-March



c) April-June

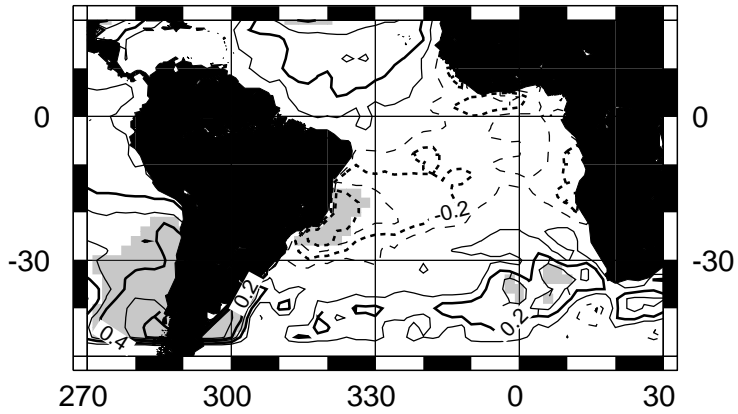


Figure 8

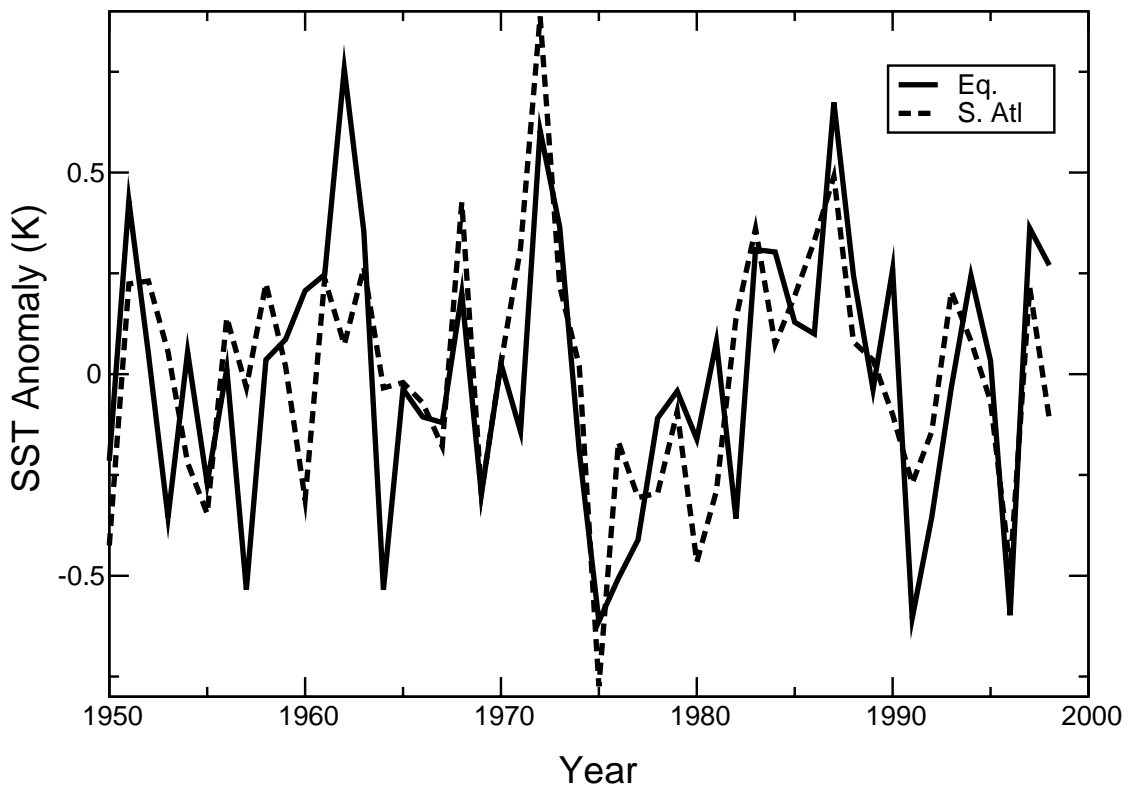


Figure 9